ELSEVIER

Cement & Concrete Composites 26 (2004) 99–111

Cement & Concrete Composites

www.elsevier.com/locate/cemconcomp

Thermal induced stress and associated cracking in cement-based composite at elevated temperatures—Part I: Thermal cracking around single inclusion

Y.F. Fu [a], Y.L. Wong [a,*], C.A. Tang [b], C.S. Poon [a]

[a] Department of Civil and Structural Engineering, The Hong Kong Polytechnic University, Hong Kong, China
[b] Lab of Numerical Test of Material Failure, Northeastern University, Shenyang 110006, China

Accepted 25 April 2003

Abstract

This paper presents the development and verification of 2-D mesoscopic thermoelastic damage model used to numerically quantify the thermal stresses and crack development of a cement-based composite subjected to elevated temperatures. The program is then used to study the thermal fracture behavior of a cement-based matrix with a single inclusion. The results show that the mechanisms of thermal damage and fracture of the composite depend on (i) the difference between the coefficients of thermal expansion (CTE) of the inclusion and the cement-based matrix, (ii) the strengths of materials, and (iii) the heterogeneity of materials at meso-scale. The thermal cracking is an evolution process from diffused damage, nucleation, and finally linkage of cracks. If the CTE of the inclusion is greater than that of the matrix, radial cracks will form in the matrix. On the other hand, inclusion cracks and tangential cracks at the interface between inclusion and matrix will form if the CTE of the inclusion is smaller than that of the matrix.

Keywords: Thermal stress; Thermal induced cracking; Heterogeneity; Numerical simulation

1. Introduction

Thermal cracking induced by thermal mismatch has been one of the problems in a cement-based composite material under elevated temperatures. For a multi-phase material, the eigenstrains deriving from the heterogeneous deformations among phase components inevitably cause cracking in the composite, even though it is under a uniform temperature field. Experimental results [1] have shown that this type of cracking significantly reduces the strength and elastic modulus of a cement-based composite. However, the entire thermal cracking process (initiation, propagation and linkage of cracks) and the associated stress distributions under elevated temperatures are difficult to quantify experimentally, mainly because of the limitation of equipment and the complex structure of a composite material.

In order to understand the failure mechanism of a composite material due to thermal effects, many mathematical models have been proposed [1–3]. In these models, the driving stresses for the crack initiation and propagation are the heterogeneous eigenstresses, which develop in and around the restraining inclusion. These eigenstresses might be caused by thermal expansion, shrinkage [4,5], initial strains and misfit strains. Timoshenko and Goodier in 1970 [6] proposed a closed-form solution for the axisymmetric problem of a circular inclusion concentrically embedded in the circular disc of another phase material with different thermal and mechanical properties. Hsueh et al. [7] transformed a composite with a microstructure of square-array, hexagon-array, brick-array grains, as well as the actual microstructure of random-array grains into a simple composite-circle analytical model. The residual thermal stresses were predicted reasonably well using the proposed linear elastic solutions except for the model microstructure of brick-array grains. A modified version of Timoshenko and Goodier's solution incorporating the longitudinal strain proposed by Gentry and Husain

* Corresponding author. Tel.: +852-2766-6009; fax: +852-2334-6389.
E-mail address: ceylwong@inet.polyu.edu.hk (Y.L. Wong).

0958-9465/$ - see front matter © 2003 Elsevier Ltd. All rights reserved.
doi:10.1016/S0958-9465(03)00086-6

Nomenclature

α	coefficient of thermal expansion	ζ	coefficient of residual strength
φ	density function of mechanical property	S	peak-strength
Φ	distribution function of mechanical property	S_r	residual strength
β	material property	S_c	uniaxial compressive strength
β_0	mean value of material property	S_t	uniaxial tensile strength
RVE	representative volume element	λ	ratio of tensile strength to compressive strength
σ	thermal stress		
D	damage variable	θ	friction angle
D_T	damage variable by temperature increment	σ_1	maximum principal stress
D_m	damage variable by thermally incompatible deformation	σ_2	minimum principal stress
		a	radium of inclusion
ε	strain induced both by internal and external restriction	b	radium of matrix
		r	distance from center of inclusion
$\varepsilon_{thermal}$	initial strain induced by temperature variation	σ_{i2}	mean strength of inclusion of Specimen no. 2
$\varepsilon_{\sigma 0}$	strain corresponding to peak-strength	σ_{i3}	mean strength of inclusion of Specimen no. 3
E^0	initial elastic modulus	σ_{i4}	mean strength of inclusion of Specimen no. 4
ΔT	temperature increment	σ_{i5}	mean strength of inclusion of Specimen no. 5

[2] was also used to study the differential pressure developed in the interface between concrete and a composite rod. As for a 40 °C temperature increase, the concrete was modeled with a linear-elastic and nonlinear tension-softening material model using a finite element approach. The calculated results showed that the large spacing of the rods and the thick concrete cover were helpful to reduce the tensile stress in concrete as well as the potential for thermally induced cracking. Based on a fracture mechanics model, Timoshenko and Goodier's solution was adopted by Dela and Stang [3] to calculate the crack growth with time in a high-shrinkage cement paste with a single aggregate disc. The experimentally measured stresses in the selected circular aggregate were employed to predict the stresses distributed in cement paste and the crack growth at a crack tip close to the aggregate in terms of a given stress intensity factor.

Although the above-mentioned models deepen the understanding on thermal stress and cracking, essentially, none of them can simulate the entire thermal cracking process from crack initiation to propagation. Hsueh's and Russell's models can determine the stress distribution around a single inclusion in the composite before crack initiates. Dela's model was suitable to calculate the critical stress value when an existing crack starts to grow. The stress distribution represented by this model would be invalid as soon as the crack is extended. A fracture mechanics model is able to study the growth of existing single crack, but it is not suitable to explain the initiation and coalescence of cracks. More importantly, the phase materials of a cement-based composite are often heterogeneous so that the effect of change in microstructure (mesostructure) on the macroscopic behavior is difficult to be studied by using an analytical model.

Consequently, a numerical method appears to be an effective tool to model cracking processes. Substantial progress [8,9] has been achieved in numerical simulation of failure occurring in a cement-based composite at ambient temperatures. However, a satisfactory model to simulate the cracking processes caused by the thermal induced stresses in a heated cement-based composite is still not available.

The aim of this paper is to propose and verify a mesoscopic thermoelastic damage (MTED) model, that can numerically simulate the formation, extension and coalescence of cracks in a cement-based composite material (cement-based matrix + aggregate inclusion), caused by the thermal mismatch of the matrix and the inclusion under uniform temperature variations and free boundary conditions. Numerical studies of the effects of the thermal mismatch between the matrix and a single circular inclusion on the stress distribution and crack development are also presented.

2. Numerical model

In the MTED model, phase materials of a composite are considered to be heterogeneous following the Weibull distribution. Tensile and shear cracking at mesoscale occur if the stress in the composite subjected to high temperatures satisfied with the failure criteria of Coulomb–Mohr with tension cutoff.

2.1. Material model

For a cement-based composite material, the phase materials are cement mortar matrix and aggregate inclusions. Although the composite material is regarded as an isotropic elastic-brittle solid at a macroscopic scale, while the individual grains in the matrix and inclusions are distinguished at microscopic or mesoscopic scales [8]. The effect of heterogeneity on the stress distribution has been studied [10], and much of the behavior observed at a macro-level can be explained in terms of the material structure at a meso-level. As a result, the matrix and the inclusions are considered as disorder solids in a meso-scale in this study.

To account for the heterogeneity of the matrix and inclusions, their statistical distributions of properties (elastic modulus, compressive strength and Poisson ratio) are assumed to follow the Weibull distribution:

$$\varphi(h,\beta) = \frac{h}{\beta_0}\cdot\left(\frac{\beta}{\beta_0}\right)^{h-1}\cdot \mathrm{e}^{-(\beta/\beta_0)^h} \tag{1a}$$

where $\varphi(h,\beta)$ is the distribution density of parameter β which is a material property (such as strength, elasticity and Poisson ratio) of a representative volume element (RVE) in the mesh divisions, and β_0 is the mean value of the material property under consideration. h is the homogeneity index of the RVE which represents the degree of homogeneity. The statistical distribution function $\Phi(h,\beta)$ is expressed by Eq. (1b) after integrating Eq. (1a):

$$\Phi(h,\beta) = 1 - \mathrm{e}^{-(\beta/\beta_0)^h} \tag{1b}$$

The randomness of the mechanical properties of RVE can be simulated using the distribution function with given parameters h and β_0, i.e. $\Phi(h,\beta_0)$. The relationship of distribution density of RVE strength and homogeneity index is shown in Fig. 1. With increasing h, the material is more homogeneous or vice versa. For instance, we consider a material with a mean strength of 200 MPa. If the material has a homogeneity index (h) of 30, the distribution probabilities $\Phi(30,200)$ will be close to zero and unity for the strengths of RVE less than 160 and 210 MPa, respectively as shown in Fig. 1b. In another case, if it has a homogeneity index (h) of 1.1, the corresponding distribution probabilities $\Phi(1.1,200)$ will become 0.54 and 0.64 for the strengths of RVE less than 160 and 210 MPa, respectively. From these strength distributions, it is evident that increasing heterogeneity of a material will increase both the difference in mechanical properties among the RVEs, and the population of the RVE with lower strengths.

The strength, elastic modulus and Poisson ratio are randomly allocated to each RVE so to account for the inherent variability in phase materials, using the Monte-Carlo method. A more detailed introduction and explanation to the material model were reported in our previous publications [11–13]. The thermal properties (CTE) of the phase materials are assumed to be uniform and location-invariant, and only depend on the individual phase.

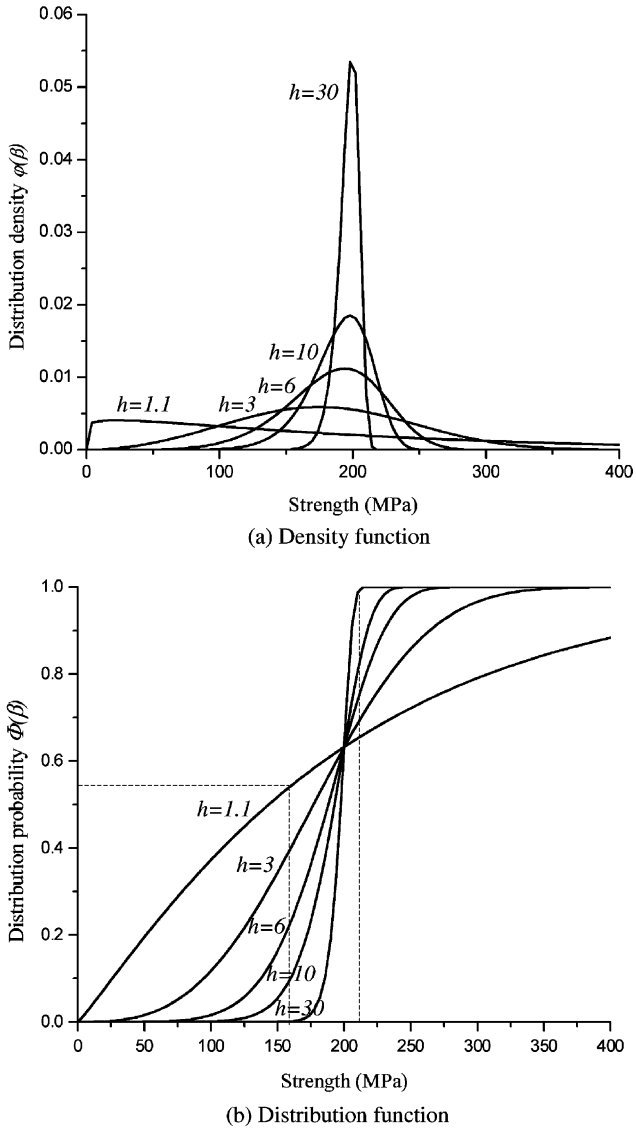

Fig. 1. Density function and distribution function of RVE strength when the mean strength is equal to 200 MPa.

2.2. Mesoscopic thermoelastic damage (MTED) model

It has been known that the thermal damages of a heated concrete is a complex problem. There are a number of affecting factors, such as thermal mismatch, temperature gradient, degradation of mechanical properties of cementitious materials due to chemical decomposition, and pore water pressure, that cause such damages. However, the focus of this paper is on the damage caused by differential thermal strains as a result

of different CTEs of the phase materials (matrix and inclusion). Studies [8,14] show that the macroscopic fracture of materials is always related to the initiation and propagation of cracks at a meso-scale. Hence, it is assumed that the damage of a cement-based composite is due to the cracking caused by thermal induced stresses at a meso-scale. The bond between the matrix and the inclusion is considered to be perfect. In fact, the proposed model can be further modified to incorporate the effects of temperature gradients and temperature-dependent mechanical properties, pending on the availability of experimental data to quantify the associated simulation functions, details of which are under investigation by the authors of this paper.

In the numerical modeling, each phase material is discretized into many RVEs with a suitable characteristic length. In general, the precision of computational results will increase with decreasing RVE size, at the expense of longer computational time. The RVE has the same size as the meshed finite element in this paper. It is also assumed that the stress–strain relationship of a RVE is linearly elastic till its peak-strength is reached, and thereafter follows an abrupt drop to its residual strength. Cracking is treated as a smeared phenomenon. That is, a crack is not considered as a discrete displacement jump, but rather changing the properties of the RVE according to a continuum law, such as damage mechanics. Although this modeling approach might appear to be crude, however, the complex failure phenomenon (such as compressive and tensile failure) and the nonlinear behavior in a macro-scale have been proved to be successfully simulated using the material heterogeneity [11]. The behavior laws of the RVE are implemented by introducing a MTED variable D into a constitutive relationship.

Based on the above-mentioned ideas and the damage mechanics [21], the general form of an effective stress for a given state of damage for a RVE can be expressed as follows:

$$\sigma = (1 - D) \cdot E^0 \cdot \varepsilon_\sigma \tag{2}$$

where σ is the effective stress, D is the damage variable, E^0 is the elastic modulus at a reference/undamaged condition (such as at reference temperature), and ε_σ is the strain. Under a uniform temperature field, the damage is induced both by differential thermal strains and by the temperature increment ΔT, the general expression of damage variable is $D = D(\varepsilon_\sigma, \Delta T)$. Let D_m and D_T denote the damages by the thermal strain and temperature increment, respectively. They can be expressed in terms of the stiffness degradation as follows:

$$D_\mathrm{m} = 1 - \frac{E(\varepsilon_\sigma)}{E^0} \tag{3}$$

$$D_\mathrm{T} = 1 - \frac{E(\Delta T)}{E^0} \tag{4}$$

where $E(\varepsilon_\sigma)$ and $E(\Delta T)$ are the elastic modulus corresponding to a given thermal strain ε_σ and the elastic modulus at temperature increment of ΔT, respectively. If they are independent, the damage variable $D(\varepsilon_\sigma, \Delta T)$ can be expressed as follow:

$$D(\varepsilon_\sigma, \Delta T) = 1 - (1 - D_\mathrm{m}) \cdot (1 - D_\mathrm{T})$$

$$D(\varepsilon_\sigma, \Delta T) = 1 - \frac{E(\varepsilon_\sigma)}{E^0} \cdot \frac{E(\Delta T)}{E^0} \tag{5}$$

Since the temperature-dependent properties are not considered, the damage D_T is equal to zero. According to the description of the damage process of a material by Mazars [14] and Yu [15], the thermal induced damage before and after the peak-strength can be determined by the thermal strain and the temperature increment ΔT

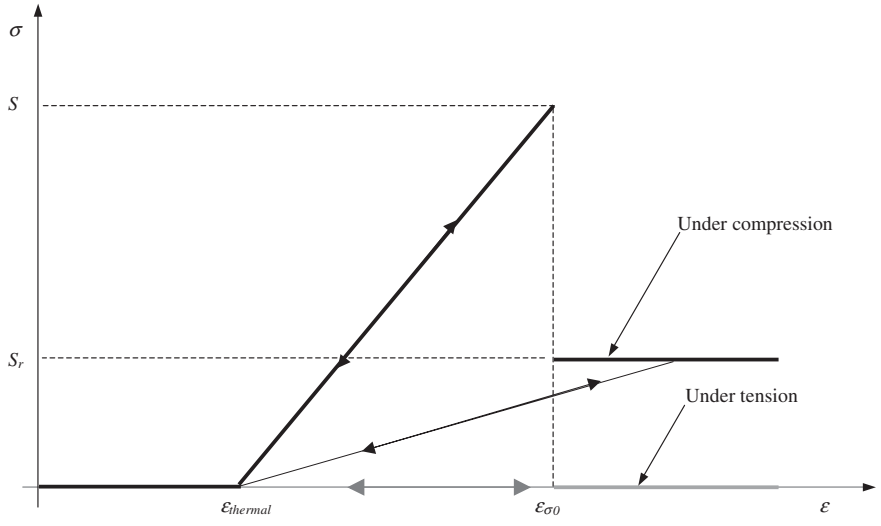

Fig. 2. Thermoelastic damage model of RVE.

through a separation function, respectively. Fig. 2 shows a general constitutive relationship of a RVE under thermal loading. At a temperature increment of ΔT, the initial thermal strain $\varepsilon_{\text{thermal}}$ is equal to $\alpha \cdot \Delta T$, and the damage at any given thermal strain can be calculated from Eq. (6)

$$D(\varepsilon, \Delta T) = \begin{cases} 0, & \varepsilon_{\text{thermal}} \leqslant \varepsilon \leqslant \varepsilon_{\sigma 0} \\ 1 - \frac{\xi(\varepsilon_{\sigma 0} - \alpha \cdot \Delta T)}{(\varepsilon - \alpha \cdot \Delta T)}, & \varepsilon \geqslant \varepsilon_{\sigma 0} \text{ under compression} \\ 1, & \varepsilon \geqslant \varepsilon_{\sigma 0} \text{ under tension} \end{cases} \tag{6}$$

where $D(\varepsilon_\sigma, \Delta T)$ represents the thermal damage with respect to the thermal strains. $\varepsilon_{\sigma 0}$ is the strain at peak-strength; ξ $(= S_r/S)$ is the coefficient of residual strength for a RVE, S and S_r are the peak-strength and residual strength, respectively. Under compression, ξ is less than 1 but greater than 0. Under tension, ξ is equal to 0. When the strain ε becomes smaller than or equal to $\varepsilon_{\sigma 0}$, the RVE is undamaged and intact, and $D = 0$. When the strain ε is larger than $\varepsilon_{\sigma 0}$, and under a compressive state, the RVE is damaged, i.e. $D > 0$, and damage variable shall be calculated by the residual strength. Under a tensile state, the RVE is fully damaged and does not sustain any load, and $D = 1$.

The behavior for a given state of thermal induced damage can be represented by

$$\sigma = [1 - D(\varepsilon_\sigma, \Delta T)] \cdot E^0 \cdot (\varepsilon_\sigma - \varepsilon_{\text{thermal}}) \tag{7}$$

Hence, substituting Eq. (6) into Eq. (7), a mesoscopic nonlocal damage model, which can describe the complete thermal induced damage process, is expressed as:

$$\sigma = \begin{cases} E^0 \cdot (\varepsilon - \alpha \cdot \Delta T), & \varepsilon_{\text{thermal}} \leqslant \varepsilon \leqslant \varepsilon_{\sigma 0} \\ \xi \cdot E^0 \cdot (\varepsilon_{\sigma 0} - \alpha \cdot \Delta T), & \varepsilon \geqslant \varepsilon_{\sigma 0} \text{ under compression} \\ 0, & \varepsilon \geqslant \varepsilon_{\sigma 0} \text{ under tension} \end{cases} \tag{8}$$

In order to simulate the thermal damage induced by thermal tensile or compressive stresses, a failure criterion, which can consider the effects of both tension and compression, is necessary. In this study, the Mohr–Coulomb criterion with tension cutoff [16] is chosen as the criterion of cracking:

$$\begin{cases} \sigma_1 - \frac{1+\text{Sin}\theta}{1-\text{Sin}\theta}\sigma_2 \geqslant S_c & \text{if } \sigma_1 \geqslant S_c\left(1 - \frac{1+\text{Sin}\theta}{1-\text{Sin}\theta} \cdot \frac{1}{\lambda}\right) \\ \text{or} & \\ \sigma_2 \leqslant -S_t & \text{if } \sigma_1 \leqslant S_c\left(1 - \frac{1+\text{Sin}\theta}{1-\text{Sin}\theta} \cdot \frac{1}{\lambda}\right) \end{cases} \tag{9}$$

where S_c and S_t are the uniaxial compressive strength and tensile strength respectively, $S_t = -\lambda \cdot S_c$, and λ is the ratio of tensile strength to compressive strength. θ is the friction angle of the material. All these parameters can be obtained experimentally. σ_1 and σ_2 are the maximum and minimum principal stresses respectively. A compressive stress is positive, and a tensile stress is negative.

Finally, a finite element program T-MFPA, incorporating the above-mentioned MTED model and failure criteria, was developed based on the Material Failure Process Analysis (MFPA) program [11,12], using a four-node isoperimetric element.

2.3. Numerical specimens

Numerical tests of five specimens (one circular specimen and four square specimens) using the T-MFPA program are reported in following sections. Let α_i denote the CTE of the inclusion and α_m be the CTE of the matrix. The specimens were analyzed under a plain stress condition without external loading.

Specimen no. 1 is a circular specimen comprising two different homogeneous phase materials (matrix and inclusion, see Fig. 3a). It is numerically heated under a uniform temperature field of 50 °C, and free boundary conditions. The numerical thermal stresses determined from the proposed program are compared with those derived from the classical theory of thermoelasticity, from which the validity of the MTED model in an elastic and undamaged state can be justified. The mechanical and geometrical properties of the phase materials are listed in Table 1. In this case, the CTE of the inclusion is greater than that of the matrix. A homogeneity index $h = 300$ is chosen so that the phase materials are basically homogeneous in nature. The numerical results are shown in the following section.

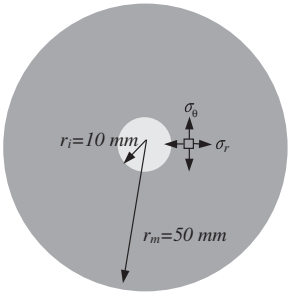

(a)

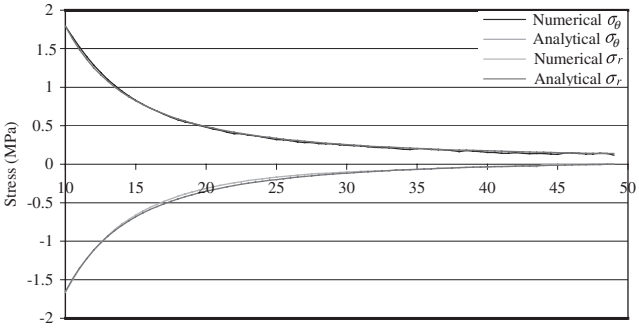

(b)

Fig. 3. Stress distribution in matrix of Specimen no. 1 at $\Delta T = 50$ °C.

Table 1
Material properties of circular Specimen no. 1

Parameter	Value	
	Matrix	Inclusion
Heterogeneity index (h)	300	300
Mean elastic modulus (MPa)	60,000	100,000
Mean compressive strength (MPa)	30	60
Poisson ratio	0.25	0.20
Coefficient of thermal expansion (/°C)	1.0E−5	1.1E−5
Temperature increment (°C)	10	10
Tension cutoff	0.1	0.1
Frictional angle (°)	30	30
Diameter (mm)	100	20
Number of elements	31,400	1256

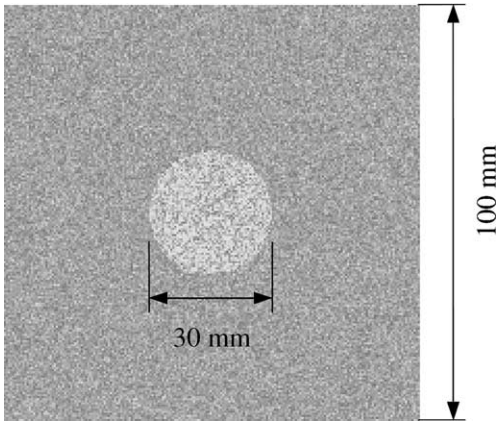

Fig. 4. Numerical square specimen with single inclusion.

Table 2
Material properties of square Specimens no. 2 to no. 5

Parameter	Value	
	Matrix	Inclusion
Heterogeneity index (h)	3	3
Mean elastic modulus (MPa)	60,000	100,000
Mean compressive strength (MPa)		
Specimen no. 2	200	300
Specimen no. 3		150
Specimen no. 4		300
Specimen no. 5		150
Poisson ratio	0.25	0.20
Coefficient of thermal expansion (/°C)		
Specimen no. 2	1.0E−5	1.1E−5
Specimen no. 3		1.1E−5
Specimen no. 4		0.9E−5
Specimen no. 5		0.9E−5
Temperature increment (°C)	10	10
Tension cutoff	0.1	0.1
Frictional angle (°)	30	30
Dimension (mm)	100×100	Φ30
Number of elements	200×200	1412

In order to determine the effects of material heterogeneity, material strength, and CTE on the stress development and the process of thermal cracking around a single inclusion, four square specimens (Specimens no. 2 to no. 5, see Fig. 4) with different thermal and mechanical properties (see Table 2) are numerically studied. Basically, the specimens can be classified into two groups. In Group 1 (Specimens no. 2 and no. 3), the CTE of the matrix is smaller than that of the inclusion. In Group 2 (Specimens no. 4 and no. 5), the CTE of matrix is larger than that of the inclusion. Within a group, the only variable is the mean strength of the inclusion. The four specimens have the same homogeneity index h equal to 3, representing a high degree of heterogeneity. They are subjected to a uniform temperature increment from 20 to 620 °C at an incremental step of 10 °C.

3. Model validation

Fig. 3b shows the comparison of the thermal stresses around the single inclusion of Specimen no. 1 calculated from the T-MFPA program, and from the analytical solutions (Eqs. (10) and (11)) derived from the classical theory of thermo-elasticity [6,17].

It is evident that under an elastic and undamaged state, an excellent agreement between the stresses obtained from the two different approaches has been obtained.

4. Thermal cracking history of square specimens

Fig. 5 shows the effect of thermal mismatch on the thermal induced damages and fracture processes of Specimen no. 2 (Group 1) and Specimen no. 4 (Group 2) due to increasing temperatures. Fig. 6 illustrates the influence of the mean strength of the inclusions on the crack development in each group. Detailed descriptions of crack formation of the specimens are shown below.

4.1. Thermal cracking in composite of $\alpha_i > \alpha_m$

In the case of Specimen no.2, since the α_i (CTE) of the inclusion is greater than that of the matrix (α_m), the incompatibility of thermal deformation at the interface between the matrix and the inclusion leads to the stress concentration around the inclusion (see Fig. 5a(a)). The inclusion is under a statistically hydrostatic compression, and the matrix is under a combination of compression and tension. When the temperature reaches 200 °C, a few broken elements randomly occur (due to heterogeneity) in the high stress zone around the inclusion. With increasing temperatures, the number of the diffused damaged elements increases. The damaged elements exist in both the high stress zone and in the low stress zone, but most of them are located near the for-

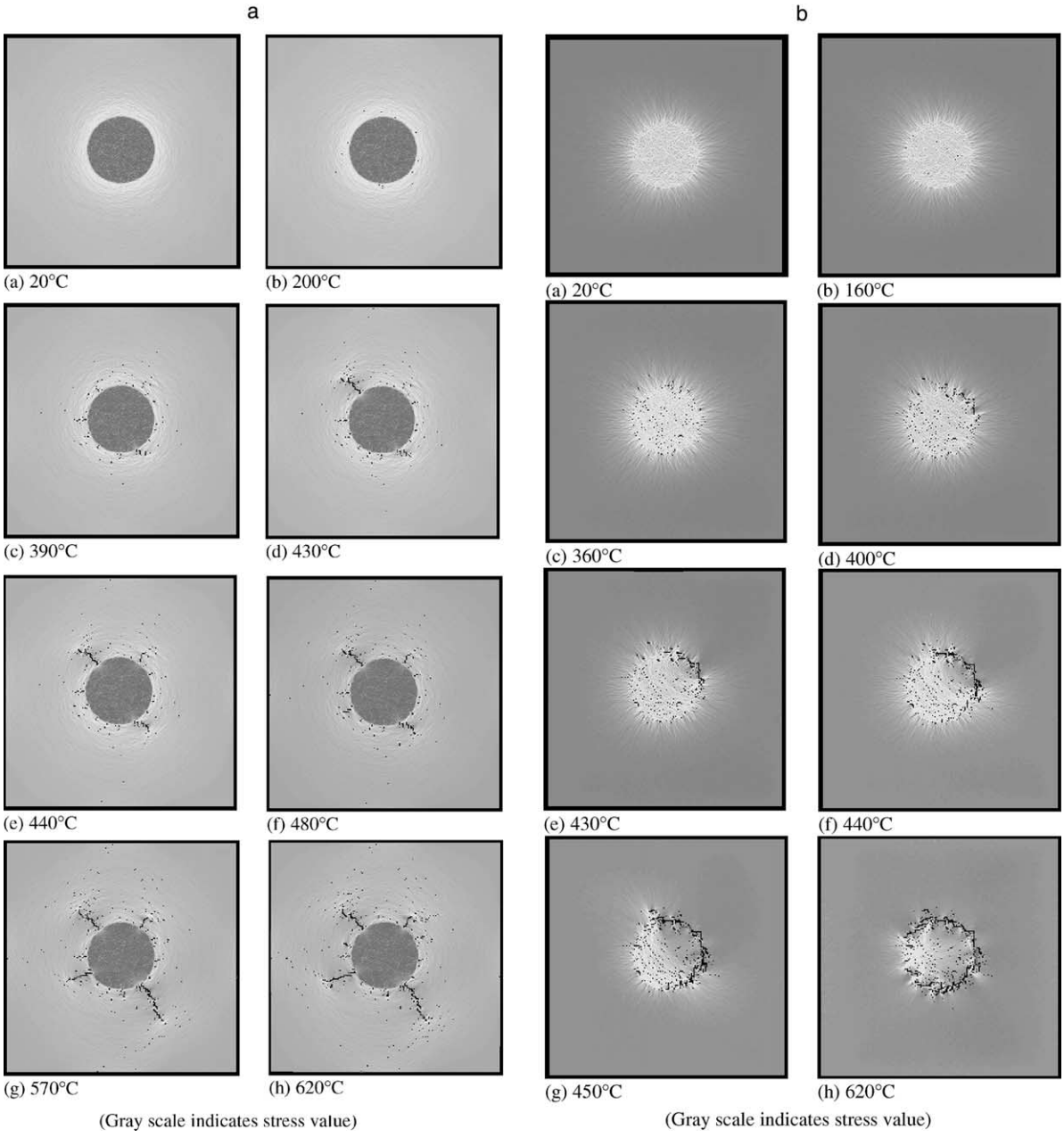

Fig. 5. (a) Thermal cracking of cement-based composite of Specimen no. 2 (inclusion diameter = 30 mm and $\alpha_i = 1.1 \times 10^{-6}$/°C). (b) Thermal cracking of cement-based composite of Specimen no. 4 (inclusion diameter = 30 mm and $\alpha_i = 0.9 \times 10^{-6}$/°C).

merly broken elements in the high stress zone (see Fig. 5a(c)). When the temperature increases to 430 °C, a macro-crack is formed firstly at the top-left area around the inclusion. At the same time, only a few of cracks nucleate far away from the high stress zone around the inclusion (see Fig. 5a(d)). As the temperature further increases, the broken elements around the inclusion nucleate into several discontinuous macro-cracks (see Fig. 5a(e) and (f)), and simultaneously corresponding tensile stress zones are formed at the tips of these cracks. Bridges are formed between the cracks due to the fact that many small cracks simultaneously grow at different locations caused by the heterogeneity. This phenomenon is also described by Van Mier [19]. As the temperature rises to 570 °C, all these macro-cracks further propagate under the tensile stresses at their tips, followed by the occurrence of dispersed damaged elements in the fracture process zone. During the heating process, the macro-cracks are formed in the way that the discontinuous cracks continue to grow and bridges are formed. The shapes of these cracks are irregular, rough and bifurcate (see Fig. 5a(e)–(h)). The macro-cracks formed along the radial direction around the inclusion can be called ''radial cracks'', which were also evident in the

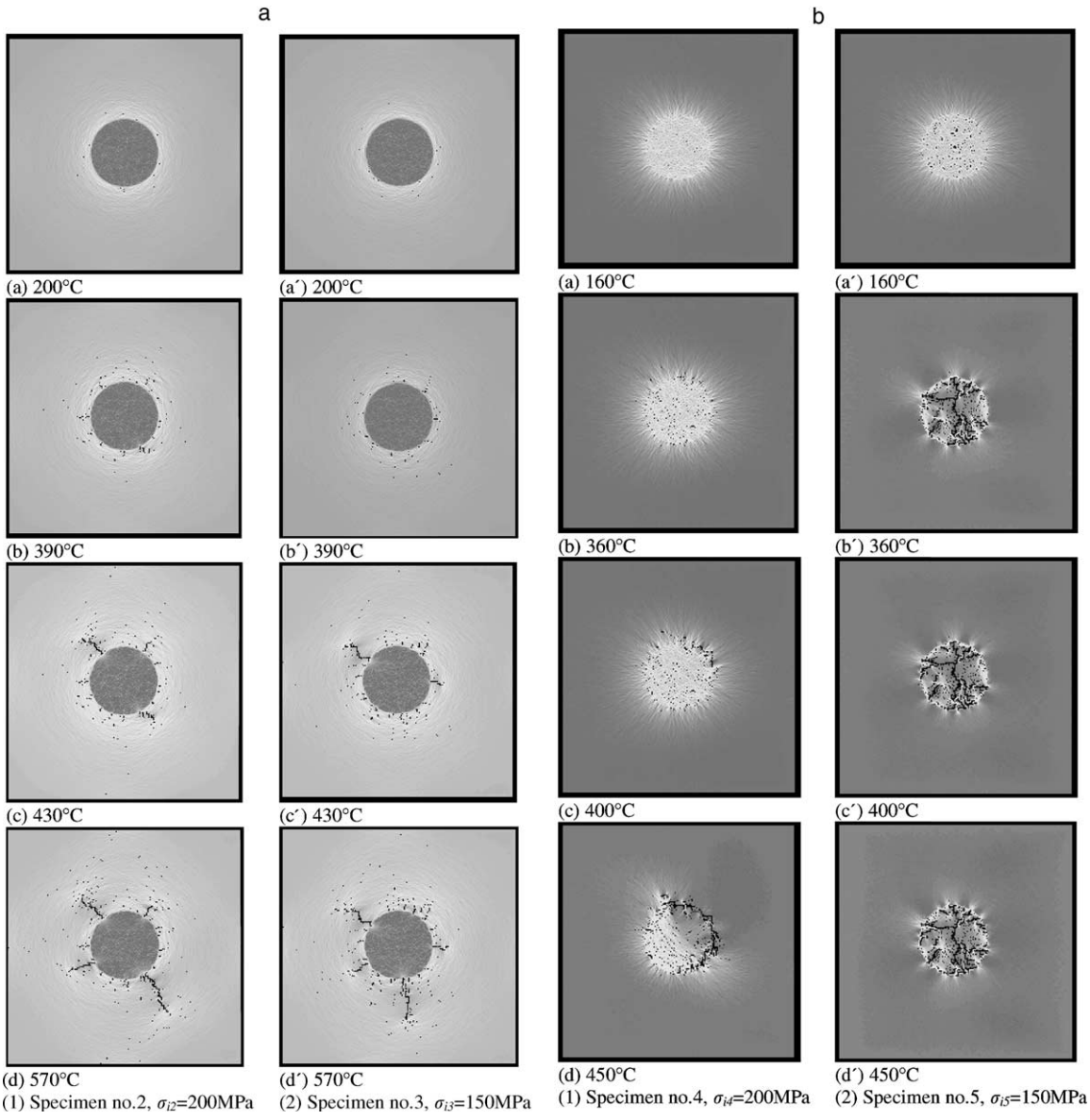

Fig. 6. (a) Thermal cracking processes of specimens in Group 1. (b) Thermal cracking processes of specimens in Group 2.

experiments reported by Zhou et al. [18] and Goltermann [5].

It is also noted that when the main macro-cracks begin to propagate, the pace of minor crack development is slow down (see Fig. 5a(g) and (h)).

Fig. 6a shows the thermal fracture process of the companion Specimen no. 3 with a lower mean strength (σ_{i3}) of the inclusion than that (σ_{i2}) in Specimen no. 2. It is evident that the variation of the mean inclusion strength does not affect the patterns of thermal damage initiation and propagation.

4.2. Thermal cracking in composite of $\alpha_i < \alpha_m$

In the case of Specimen no. 4, since the α_i (CTE) of the inclusion is smaller than that of the matrix (α_m), a zone of stress concentration also occurs around the inclusion. The inclusion is stressed under tension and the matrix is under a combination of tension and compression (see Fig. 5b(a)). When the temperature reaches 160 °C, a few of the damaged elements distribute disorderly inside the inclusion. With increasing temperatures, the number of broken elements grows, and a few of them occur in the stress concentration zone outside the inclusion (see Fig. 5b(c)). When the temperature increases to 400 °C, the broken elements at the interface between the matrix and the inclusion nucleate and form several small discontinuous cracks. As the temperature becomes further higher, the discontinuous cracks at the interface propagate gradually and coalesce with the stress transferring from the inclusion and the matrix nearby the inclusion to the tips of the cracks (see Fig.

5b(e)–(g)). Eventually, after the temperature has reached 620 °C, most of all the elements around the interface between the matrix and the inclusion are broken and a nearly close circular macro-crack is formed at the interface. The high stress distributing inside the inclusion is transferred into the crack tips. This kind of crack is called ''tangential crack'', which is also observed in the experiments by Zhou et al. [18] and Goltermann [5].

Fig. 6b demonstrates the thermal fracture process of the companion Specimen no. 5 with a lower mean strength (σ_{i5}) inclusion than that (σ_{i4}) in Specimen no. 4. Although the thermal damage initiation and crack propagation of the two specimens are similar, the number of the broken elements and the kinds of cracks at each temperature level are different. At a lower temperature, more elements in the inclusion of Specimen no. 5 are damaged than those in Specimen no. 4 (see Fig. 6b(a) and (a′)). When the temperature reaches 360 °C, the macro-cracks pass through partly or wholly the inclusion, and high stresses previously distributed around the inclusion are transferred into the tips of these cracks (as shown in Fig. 6b(b′)). With increasing temperatures, these discontinuous cracks nucleate and coalesce with the redistributing stress field (as shown in Fig. 6b(c′) and (d′)). This kind of crack occurred inside the inclusion is called ''inclusion crack''.

5. Thermal stress fields of square specimens

5.1. Effect of thermal mismatch

Although the four specimens are subjected to uniform temperature changes, local stress concentration occurs around the inclusion due to the thermal mismatch between the matrix and the inclusion.

When the CTE of the inclusion is greater than that of the matrix, the inclusion in Specimen no. 2 is stressed under a state of statistically hydrostatic compression due to the restriction from the matrix, and the matrix is under a general bi-axial state of stresses (tensile/compressive and shear stresses) due to the outward expansion from the inclusion. The distribution of maximum and minimum principal stresses and the maximum shear stress along the mid-section of Specimen no. 2 can be shown in Fig. 7a(a). Although the maximum and minimum principal stresses in the inclusion are high, the maximum shear stress is much smaller so that few elements with lower strength in this area reach their failure strength. The absence of tensile stresses in the inclusion delays the attainment of the Mohr–Coulomb with tension cutoff failure criterion. Unless the inclusion is abnormally weak in compression, the strength of inclusion has no effect on damage initiation (see Fig. 6a). As a result, most of the diffused damages distribute in the high stress zone of the matrix around the inclusion for Group 1 specimens. With increasing temperatures, these broken elements nucleate and form several discontinuous cracks due to the stress redistribution at the crack tips. Since the minimum principal stress is nearly perpendicular to the radial direction of the inclusion and is in tension, these cracks are developed in the manner of radial cracks in the matrix.

When the CTE of the inclusion is smaller than that of the matrix, the inclusion in Specimen no. 4 is stressed under bi-axial tension, and the matrix remains in a state of compressive/tensile and shear stresses (see Fig. 7b). Since a bi-axial tension leads to early attainment of the failure criterion, it is not surprised that the initiation of damage takes place only in the inclusion of Group 2 specimens. In such a case, the strength of the inclusion has considerable effects on the crack formation. That is, a weaker inclusion will have damage initiated at a lower temperature and grow more rapidly at high temperatures (see Fig. 6b). The minimum principal stress in the matrix is parallel to the radius direction of the inclusion and is in tension, so that the main cracks propagate in the manner of tangential cracks at the matrix–inclusion interfacial region.

5.2. Effect of heterogeneity at meso-scale

The thermal stress fields are shown in Figs. 4–6. The bright color indicates the higher stress, and vice versa. It is found that the points with different scale colors exist in a same zone. It means that there are existing points subjected to different stresses due to the heterogeneity at meso-scale in such zone, where the stress field is statistically uniform at macro-scale. The ratio of the local stress to the local strength is a very important parameter which can be used to decide whether or not an element fails. The effect of the heterogeneity at meso-scale can be reflected by the stress fluctuation shown in Fig. 7. In comparison with the results from Fig. 3, the curves of stress distribution along the mid-section E–E in Specimens no. 2 to no. 5 before crack initiating are characterized by an irregular variation of stress values (see Fig. 7a and b). Such a strong thermal stress fluctuation in a heterogeneous composite, which can be quantitatively identified in our numerical study, is difficult to be determined by experiments.

Taking into account of the material heterogeneity, the failure of a material is dependent both on the induced stress level and on the strength itself. An element subjected to high stress may not break due to the fact that this element has higher strength; whereas an element subjected to low stress may break because of its low strength. These kinds of failure are definitely different, since their released energies are different. Consequently, some RVE can still remain un-fractured in a zone of high stress, if these elements have higher

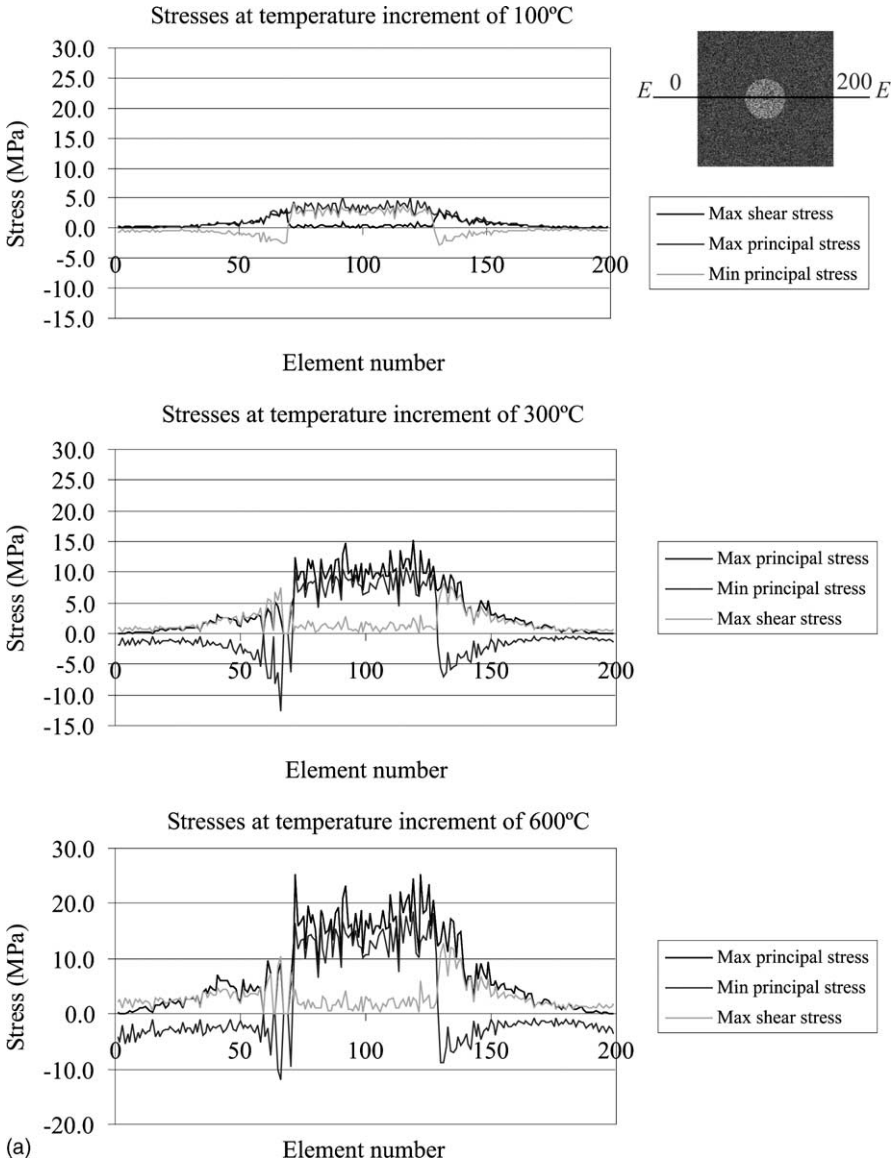

Fig. 7. (a) Distribution of σ_1, σ_2 and τ along mid-section E–E in Specimen no. 2. (b) Distribution of σ_1, σ_2 and τ along mid-section E–E in Specimen no. 4.

strength than others due to the heterogeneity of material properties. This phenomenon, that damage initiates randomly, has been experimentally demonstrated in some previous studies [20].

When a RVE with high strength is located at the crack tip, the element does not fracture and resists the crack propagation. The crack deviation and meandering due to elements with higher strength blocking the path of a crack produce an irregular crack path and echelons, which can be observed in Fig. 5. This may also significantly increase the crack length and the fracture energy. Based on this mechanism of crack linkage, a few damaged regions may eventually become dominant and form macro-cracks, while the other small cracks or damaged elements stop growing, i.e. the formation of main macro-cracks is capable of shielding the further development of the cracks in less damaged regions (as shown in Fig. 5a(g) and (h)).

5.3. Effect of mean strength of inclusion

In Specimen no. 3, the inclusion is under statistically hydrostatic compression. Although the mean strength (σ_{i3}) of the inclusion is less than that (σ_{i2}) of the inclusion of Specimen no. 2, the fractures mainly distribute in the matrix subjected to the tensile stress field.

In Specimen no. 5, the inclusion is subjected to a tensile stress field. Since the mean strength (σ_{i5}) of the inclusion is smaller than that (σ_{i4}) of the inclusion of Specimen no. 4, the ratio of the local stress to the local strength for a given element inside the inclusion is increased in Specimen no. 5. As a result, nearly all the

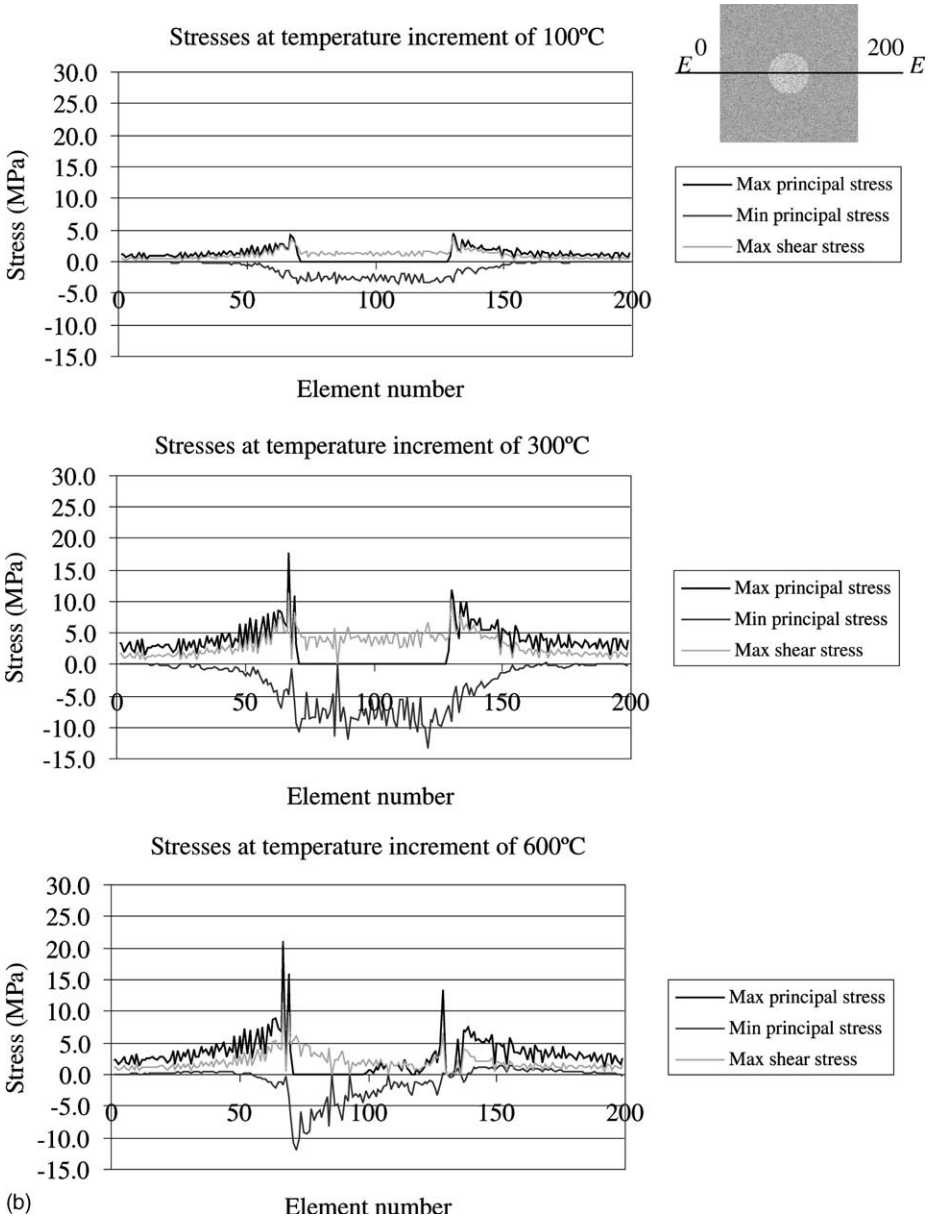

Fig. 7 (*continued*)

fractures and main cracks distribute in the inclusion in Specimen no. 5. This is why the cracks propagate only inside the inclusion.

6. Thermal crack patterns

Three types of thermal cracks have been identified: radial cracks, tangential cracks and inclusion cracks, in a cement-based composite. All these cracks are schematically shown in Fig. 8. The formation and propagation of these cracks are dependent on the difference in CTE between the inclusion and the matrix. Although all these cracks are located in different places, all of them are produced by the tensile eigenstresses derived from the thermal mismatch. From the consideration of the eigenstresses, the thermal crack patterns numerically obtained have a good agreement with those experimentally determined [5]. The crack patterns observed can be used to determine the possible mechanism of thermal failure of the mortar matrix and the aggregate inclusion used in concrete.

The relation of the crack length and the temperature is shown in Fig. 9. In Specimens no. 2 and no. 3, the crack lengths are dictated by radial cracks, and they steadily increase with temperatures. However, in Specimens no. 4 and no. 5, the crack lengths, mainly contributed by tangential and inclusion cracks, suddenly increase at 200 and 400 °C, respectively. In the situation of Specimen no. 5, the sudden increase of crack length is

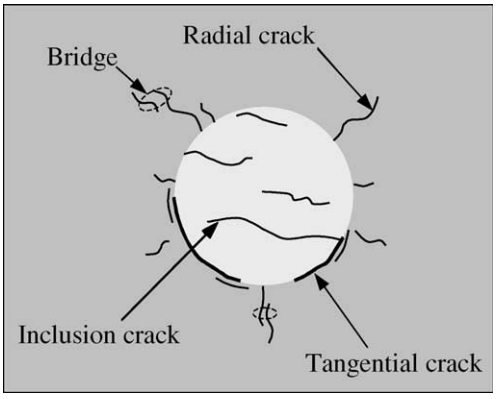

Fig. 8. Schematic of three types of crack patterns.

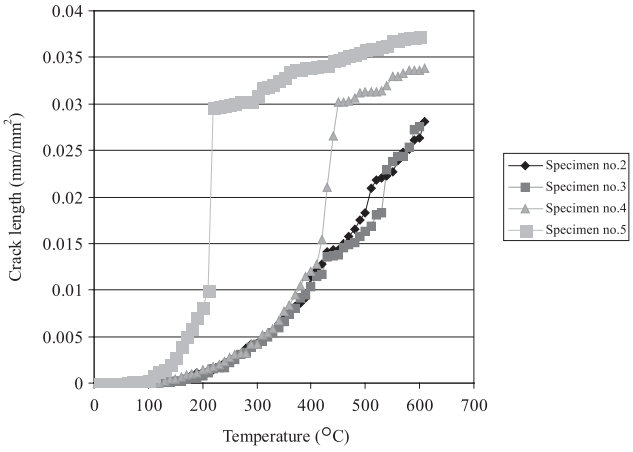

Fig. 9. Relation between crack length and temperature.

possibly caused by the low mean strength of the inclusion.

7. Conclusions

In this paper, a MTED model was formulated and then incorporated in the established MFPA program for the simulation of the crack formation, extension and coalescence in a cement-based composite (aggregate inclusion + cement mortar matrix) at elevated temperatures. Based on the studies of four specimens, some fundamental characteristics of thermal cracks, caused by different CTE of the inclusion and the matrix, are summarized as follows:

(1) When the CTE of the inclusion is greater than that of the matrix, the stress field in the inclusion is statistically hydrostatic compression, and that in the matrix is a combination of compression and tension. As the temperature increases, the damage is intensified resulting in crack formation and extension in the matrix only. Radial cracks propagate from the matrix–inclusion interface outwards. The strength of the inclusion has a little effect on crack development. When the CTE of the inclusion is smaller than that of the matrix, the inclusion is stressed in tension, and the matrix is in compression/tension. The tangential cracks are formed along the interface between the matrix and the inclusion. The increase in the strength of the inclusion retards the growth of damage and cracks in the inclusion at higher temperatures. The cracks so created are inclusion cracks in the inclusion.
(2) Damage will initiate in the matrix for the composite, in which the CTE of inclusion is greater than that of the matrix. Damage initiates both in the matrix and in the inclusion for the composite, in which the CTE of inclusion is less than that of the matrix. The random distribution of damage is dominated by the heterogeneity at meso-scale.
(3) The initial damage is caused not only by the high local stress but also by the low local strength. The ratio of the local stress to the local strength is a very important parameter to decide whether an element reaches a failure state.
(4) When a crack tip encounters a RVE with higher elastic modulus and strength, the prevailing direction of crack propagation will be obstructed. The crack will further extended in another direction or nucleated in other locations to avoid this element. This produces an irregular crack path and echelons. Hence, heterogeneity increases the fracture energy of the material. The formation of macro-cracks in a damaged region will shield the development of smaller cracks in a less damaged region.

In this paper, the thermal cracking process around a single inclusion is simulated numerically, and the dependence of the failure mechanism on the thermal mismatch and heterogeneity is studied. In order to study the interactions of multi-inclusions, including random-array irregular inclusions on the thermal cracking of a cement-based composite, another series of detailed numerical simulations using the proposed T-MFPA program have been conducted, details of which will be presented in the companion (Part II) paper.

Acknowledgements

The materials presented in this paper are some of the findings of the G-V848 research project entitled "Thermal Stress and Associated Damage in Concrete at Elevated Temperatures" of The Hong Kong Polytechnic University. The project is also partly supported by the NNSF of China (No. 50174013).

References

[1] Kristensen L, Hansen TC. Cracks in concrete core due to fire or thermal heating shock. ACI Mater J 1994;91(5):453–9.

[2] Gentry TR, Husain M. Thermal compatibility of concrete and composite reinforcements. J Compos Construct 1999;3(2):82–6.

[3] Dela BF, Stang H. Two-dimensional analysis of crack formation around aggregates in high-shrinkage cement paste. Eng Fract Mech 2000;65:149–64.

[4] Goltermann P. Mechanical predictions on concrete deterioration. Part 1: Eigenstresses in concrete. ACI Mater J 1994;91(6):543–50.

[5] Goltermann P. Mechanical predictions on concrete deterioration. Part 2: Classification of crack patterns. ACI Mater J 1995;92(1):58–63.

[6] Timoshenko SP. Theory of elasticity. 3rd ed. New York: McGraw-Hill; 1987.

[7] Hsueh CH, Becher PF, Sun EY. Analysis of thermal expansion behavior of intergranular two-phase composites. J Mater Sci 2001;36:255–61.

[8] Van Mier JGM. Fracture processes of concrete: assessment of material parameters for fracture models. Boca Raton, FL: CRC Press; 1997.

[9] Mohamed AR, Hansen W. Micromechanical modeling of concrete response under static loading—Part I: Model development and validation. ACI Mater J 1999;96(2):196–203.

[10] Brandt AM. Cement-based composites: materials, mechanical properties and performance. UK: E & FN Spon; 1995.

[11] Tang CA. Numerical simulation of progressive rock failure and associated seismicity. Int J Rock Mech Min Sci 1997;34(2):249–62.

[12] Fu YF. Study of rock failure process by numerical testing. MSc thesis. Shenyang, China, Northeastern University, 1997 [in Chinese].

[13] Fu YF, Tang CA. Numerical simulation on influence of mesoscopic heterogeneity on macroscopic behavior of rock failure. Chinese J Geotech Eng 2000;22(6):705–10 [in Chinese].

[14] Mazars J. A description of micro- and macro-scale damage of concrete structures. Eng Fract Mech 1986;25(5/6):729–37.

[15] Yu TQ. Linear damage model of separation function for concrete. Fract Strength Rock Concrete 1982;2:14–6 [in Chinese].

[16] Jaeger JC, Cook NGW. Fundamentals of rock mechanics. 2nd ed. London: Chapman & Hall; 1976.

[17] Boley BA, Wiener JH. Theory of thermal stresses. New York: John Wiley; 1960.

[18] Zhou YC, Song SG, Duan ZP, Hashida T. Thermal damage in particular—reinforced metal matrix composites. J Eng Mater Technol 2001;123:251–60.

[19] Van Mier JGM. Mode I fracture of concrete: discontinuous crack growth and crack interface grain bridging. Cement Concrete Res 1991;21:1–15.

[20] Mogi K. Earthquake prediction. Japan: Academic Press; 1985.

[21] Krajcinovic D. Damage mechanics. The Netherlands: Elsevier Science Publishers; 1996.